Inorganic Chemistry

pubs.acs.org/IC

Article

Binary Intermetallics in the 70 atom % R Region of Two R−Pd Systems (R = Tb and Er): Hidden, Obscured, or Nonexistent?

Thomas Bell, Volodymyr Smetana, Anja-Verena Mudring,* and Gerd H. Meyer*

Cite This: *Inorg. Chem.* 2020, 59, 10802−10812

Read Online

ACCESS | Metrics & More | Article Recommendations | Supporting Information

ABSTRACT: Although rare-earth-metal−transition-metal (R/T) phase diagrams have been explored extensively, our recent studies have uncovered new previously nonexistent binary intermetallics. These compounds belong to a narrow region between 70 and 71.4 atom % of the rare-earth metal but represent four different structure types. The binaries Tb_7Pd_3 and $Er_{17}Pd_7$ are compositionally approaching (less than 1 atom % difference) the previously reported $R_{2.16}Pd_{0.89}$ (R = Tb and Er), and apparently form by peritectoid transformation, thus, being hard to detect by fast cooling. Tb_7Pd_3 (**1**) crystallizes in the Th_7Fe_3 structure type (*hP*20, $P6_3mc$, a = 9.8846(4) Å, c = 6.2316(3) Å, Z = 2) while $Er_{17}Pd_7$ (**2**) belongs to the $Pr_{17}Co_7$ type being its second reported representative (*cP*96, $P2_13$, a = 13.365(2) Å, Z = 4). $Er_{17}Pd_7$ (**2**) is overlapping with the cubic *F*-centered $Er_{2.11}Pd_{0.89}$ (**3b**, $Fd\bar{3}m$, a = 13.361(1) Å, Z = 32) with practically identical unit cell parameters but a significantly different structure. Electronic structure calculations confirm that heteroatomic R−T bonding strongly dominates in all structures; T−T bonding interactions are individually strong but do not play a significant role in the total bonding.

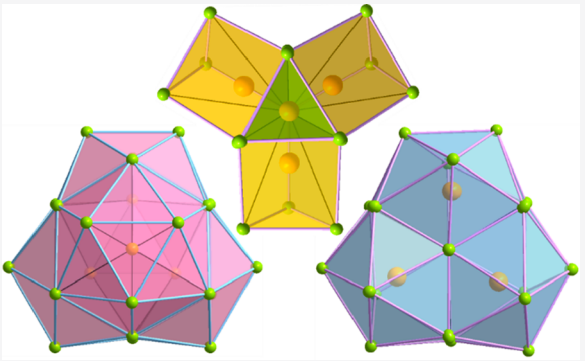

INTRODUCTION

In order to further explore cluster complex halides $\{T_tR_r\}X_x$ with group 8−10 transition metals as the endohedral atom, a systematic study of the R/T/X systems (R = rare earth metal, T = transition metal, X = Cl, Br, and I) has been performed.[1−4] When the electronegativity of the halide increases, there is an increasing competition in the formation of cluster complex halide $\{T_tR_r\}X_x$ versus intermetallic $\{T_tR_r\}$ and salt RX_3. For each specific R/T combination this competition reveals itself differently; for example, during the attempted synthesis of $\{PtPr_3\}Cl_3$ the intermetallic Pt_3Pr_4 as well as remaining $PrCl_3$ starting material was obtained. The latter was apparently working as a flux for the crystal growth of the intermetallic. A similar outcome has been observed for the synthesis targeting $\{CoPr_3\}Br_3$ leading to the formation of Co_7Pr_{17}.[5] It is interesting to note that the corresponding binary intermetallic systems, Pr/Pt and Pr/Co, have been investigated thoroughly,[6] yet neither Pr_4Pt_3 nor $Pr_{17}Co_7$ had been identified during the initial phase diagram constructions. Note that from here on the notation R/T is adopted which is more common in the intermetallics community.

Nevertheless, binary rare-earth-metal−transition-metal systems, R−T, were indeed the subject of extensive explorations not the least due to a variety of exceptional properties of the formed compounds that found their applications particularly as magnetic materials and for hydrogen storage ($LaNi_5$).[8,9] Even though the systems were well-screened, new representatives appear from time to time, of which only the systems Pr/Pt, R/Pd, Y/Au, and Gd/Ni shall be mentioned.[7,10−13] Many of the newly discovered compounds undergo peritectoid (Pr_4Pt_3 and R_3Pd_5) or eutectoid (Gd_3Ni_2) decomposition, thus being hard to observe, while others were detected but never characterized. Our recent study on the Pr/Pt system showed that the application of various fluxes may lead to the discovery of hardly accessible or metastable intermetallics; hence, they may be hidden or obscured and have been nonexistent to that point.[10]

Both the Tb/Pd and Er/Pd systems have been explored since the 1950s exhibiting nine binary phases plus two high-temperature modifications each.[6,7] It is also worth noting that both systems are almost identical excluding the newly explored region. The systems include RPd_7 (12.5 atom % R), RPd_3 (25), $R_{10}Pd_{21}$ (32.3), R_3Pd_5 (37.5), R_2Pd_3 (40, LT and HT), R_3Pd_4 (42.9), RPd (50, LT and HT), R_3Pd_2 (60), and so-called R_5Pd_{2-x} (≥70 atom %).[7,14−28] Several attempts have been made to clarify the composition(s) and crystal structure(s) of "R_5Pd_{2-x}", an apparently congruently melting "phase", not too far away in composition from the neighboring R_3Pd_2 phases into which we shed some further light recently

Received: May 3, 2020
Published: July 15, 2020

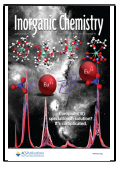

https://dx.doi.org/10.1021/acs.inorgchem.0c01311
Inorg. Chem. 2020, 59, 10802−10812

Table 1. Crystallographic Details and Refinement Parameters for Tb_7Pd_3, $Er_{17}Pd_7$ and $Er_{2.11}Pd_{0.89}$

	Tb_7Pd_3 (1)	$Er_{17}Pd_7$ (2)	$Er_{2.11}Pd_{0.89}$ (3b)
form. wt., g/mol	807.55	3588.22	447.61
space group, Z	$P6_3mc$ (186), 2	$P2_13$ (198), 4	$Fd\bar{3}m$ (227), 32
a, Å	9.8846(4)	13.3645(3)	13.361(1)
c, Å	6.2316(3)		
V, Å^3	527.29(4)	2387.03(9)	2385.1(6)
temperature, K	293(2)	293(2)	293(2)
radiation	Mo Kα	Mo Kα	Mo Kα
density (calculated), g/cm^3	9.017	9.985	9.972
absorption coefficient, μ, mm^{-1}	51.160	64.083	63.806
F (000)	1186	5912	5901
θ range for data collection, deg	2.38 to 29.04	2.16 to 26.72	2.64 to 29.94
	$-13 < h < 13$	$-16 < h < 16$	$-8 < h < 18$
index ranges	$-13 < k < 13$	$-16 < k < 16$	$-17 < k < 18$
	$-8 < l < 8$	$-16 < l < 16$	$-18 < l < 12$
intensity data collected	9622	36138	2602
number of independent reflections	552	1698	198
R_{int}; R_σ	0.1328; 0.0341	0.1027; 0.0249	0.0575; 0.0252
completeness, %	100	99.7	100
Flack parameter	0.03(5)	0.00(1)	
data/restraints/parameters	552/0/23	1698/0/77	198/0/17
goodness-of-fit (F^2)	1.203	1.134	1.096
R_1; wR_2 [$I_0 > 2\sigma$ (I)]	0.0250; 0.0676	0.0254; 0.0637	0.0337; 0.0638
R_1; wR_2 (all data)	0.0251; 0.0676	0.0255; 0.0638	0.0430; 0.0672
largest diff. peak and hole [e/Å^{-3}]	1.265 and −1.09	1.145 and −1.085	3.183 and −2.615

Table 2. Atomic Positions and Equivalent Displacement Parameters for Tb_7Pd_3, $Er_{17}Pd_7$ and $Er_{2.11}Pd_{0.89}$

		atomic parameters				
atom	Wyckoff site	x	y	z	U_{eq}	SOF
			Tb_7Pd_3 (1)			
Tb1	6c	0.12486(6)	1 − x	0.6923(1)	0.0225(3)	
Tb2	6c	0.46022(6)	1 − x	0.3041(1)	0.0233(3)	
Tb3	2b	2/3	1/3	0	0.0225(4)	
Pd	6c	0.80968(9)	1 − x	0.7559(3)	0.0257(4)	
			$Er_{17}Pd_7$ (2)			
Er1	12b	0.0108(1)	0.4931(1)	0.31664(8)	0.0239(2)	
Er2	12b	0.0136(1)	0.30950(8)	0.49317(9)	0.0237(2)	
Er3	12b	0.06630(9)	0.7447(1)	0.25583(9)	0.0249(3)	
Er4	12b	0.15081(9)	0.15238(8)	0.34692(8)	0.0267(3)	
Er5	12b	0.25835(9)	0.56362(9)	0.26025(9)	0.0236(3)	
Er6	4a	0.55530(9)	x	x	0.0286(4)	
Er7	4a	0.4024(1)	x	x	0.0287(4)	
Pd1	12b	0.1887(1)	0.3597(2)	0.3610(1)	0.0284(4)	
Pd2	12b	0.0940(2)	0.5825(2)	0.1191(2)	0.0323(5)	
Pd3	4a	0.1383(1)	x	x	0.0291(7)	
			$Er_{2.11}Pd_{0.89}$ (3b, origin at $\bar{3}m$)			
Er1	48f	0.43916(7)	1/8	1/8	0.0123(4)	
Er2	32e	0.0232(1)	0.0232(1)	0.0232(1)	0.0205(6)	0.5[a]
Er3	32e	0.1793(5)	0.1793(5)	0.1793(5)	0.012(3)	0.110(6)
Pd	32e	0.2240(2)	0.2240(2)	0.2240(2)	0.056(1)	0.890(6)

[a]Fixed occupation.

for R = Tb and Er.[29] In this article, we attempt to elucidate the formation of binary intermetallics in the narrow but obviously structurally fruitful and diverse area around 70 atom % of the rare earth element.

EXPERIMENTAL SECTION

Synthesis. Starting materials were Pd powder (99.999%), Tb and Er filings (99.9%), and RCl_3. The rare-earth halides were obtained via the ammonium chloride route from the respective oxide.[30,31] Due to the high sensitivity of some starting materials and products to moisture or air, all samples between 250 and 500 mg were weighed and loaded into tantalum ampules inside an argon-filled glovebox. Ampules were arc-sealed under helium, followed by sealing in evacuated silica tubes. Samples were placed in a furnace following the heat treatments described below.

Tb_7Pd_3 (1) and $Er_{17}Pd_7$ (2). Single crystals were grown from a melt of Pd, Tb/Er, and $TbCl_3$/$ErCl_3$ in a 1:4:4 ratio, originally

https://dx.doi.org/10.1021/acs.inorgchem.0c01311
Inorg. Chem. 2020, 59, 10802−10812

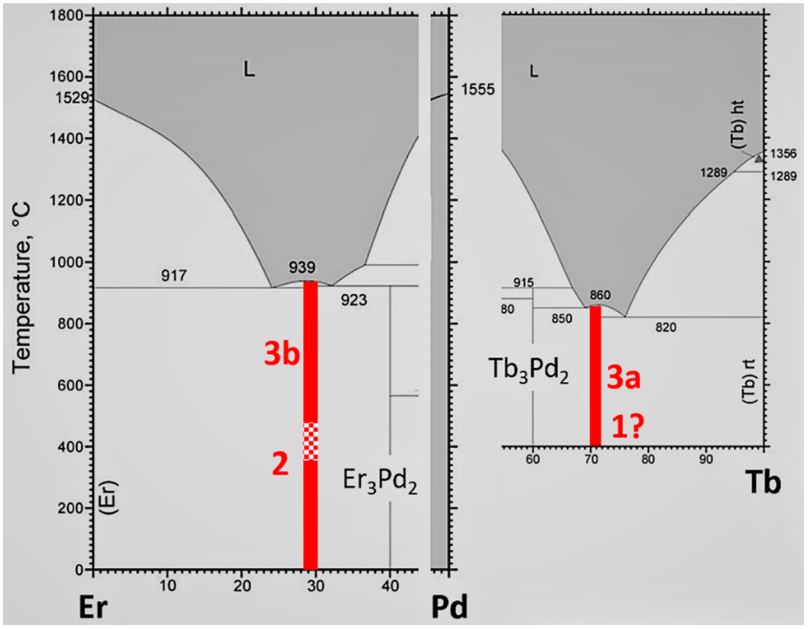

Figure 1. Parts of the binary phase diagrams for the Er/Pd and Pd/Tb systems exhibiting, in red, the +70 atom % R region. **1** and **2** could so far be obtained only in the presence of a halide flux. The red/white checkered area in the Er/Pd phase diagram highlights the region where subsequent exothermic/endothermic effects are observed upon heating by differential scanning calorimetry (DSC), see Figure 2.

targeting $\{PdR_4\}Cl_4$. The sample was prereacted at 1050 °C for 100 h, slowly (1 °C·h^{-1}) cooled to 900 °C, annealed for 150 h, cooled to 650 °C (1 °C·h^{-1}) and followed by a rate of −10 °C·h^{-1} until room temperature was reached. After the final composition had been established by single-crystal X-ray diffraction analyses (SXRD, see below), stoichiometric loadings of the starting materials corresponding to "$Er_{17}Pd_7$" have been prepared without the halide flux to obtain single-phase material. Following the initial reaction at 1050 °C for 2 days the sample was cooled at 10 °C·h^{-1} to 800 °C, subsequently annealed for 7 days, and cooled to room temperature by switching off the power to the furnace. The resulting product has been found to be phase-pure **3b**, $Er_{2.11}Pd_{0.89}$ (Figure S1).

Structure Analysis. Powder and single-crystal X-ray diffraction were used to characterize all products. Ternary samples containing metal chlorides were handled in a glovebox, while the binary intermetallic samples could be handled in air due to the low sensitivity to oxidation or hydrolysis in a laboratory environment for extended periods. A portion of the sample was ground to a fine powder for phase analysis. Powders were sandwiched between greased Mylar sheets housed by an aluminum holder. Data were gathered on a STOE STADI P image plate diffractometer (Cu Kα_1 radiation, λ = 1.54056 Å; Si external standard, a = 5.4308(1) Å) and analyzed using WinXPow software. Single-crystal X-ray diffraction was performed on a Bruker APEX CCD and Bruker VENTURE diffractometer (both Mo Kα radiation, λ = 0.71073 Å). The raw frame data were collected using the Bruker APEX3 program,[32] while the frames were integrated with the Bruker SAINT[33] software package using a narrow-frame algorithm integration of the data and were corrected for absorption effects using the multiscan method (SADABS).[34] All atom positions were refined anisotropically. Initial models of the crystal structures were first obtained with the program SHELXT-2014[35] and refined using the program SHELXL-2014[36] within the APEX3 software package. Compounds **1** and **2** have been refined as optical twins. The final coordinates were standardized with the program Structure Tidy.[37] Refinement details and structural parameters can be found in Tables 1 and 2.

Differential Scanning Calorimetry (DSC). DSC measurements have been performed under Ar flow using STA 449 F1 Jupiter, NETZSCH, on an annealed $Er_{17}Pd_7$ sample kept at room temperature for at least 3 months. The sample was placed inside a closed alumina crucible, heated to 650 °C and cooled to 150 °C at 10 °C/min.

Electronic Structure Calculations. DFT-based electronic structure calculations for $Er_{17}Pd_7$ and Tb_7Pd_3 were accomplished according to the linear muffin−tin−orbital (LMTO) method in the atomic sphere approximation (ASA).[38,39] The Wigner−Seitz radii were automatically generated and empty spheres were included for better approximation of full potentials. Basis sets of Tb 6s,(6p),5d, Er 6s,(6p),5d, and Pd 5s,5p,4d were employed. 6p orbitals of the rare-earth elements were downfolded.[40] Chemical bonding analysis was performed based on the crystal orbital Hamilton populations (COHP).[41]

RESULTS AND DISCUSSION

Two new rare earth-rich binary compounds with the late transition metal palladium, Tb_7Pd_3 (**1**, 70 atom % Tb) and $Er_{17}Pd_7$ (**2**, 70.8 atom % Er), have been observed during the exploration of rare-earth metal cluster complex halides with the endohedral transition metal atom Pd. The experiments were originally targeted at $\{PdR_4\}Cl_4$. Thus, molar mixtures of, for the example of **1**, 4$TbCl_3$ + 8Tb + 3Pd were loaded which apparently resulted in the formation of Tb_7Pd_3 + Tb + 4$TbCl_3$ where $TbCl_3$ acted as a flux for the formation of the intermetallic **1**.

Previous detailed analyses of the phase diagrams of Tb/Pd as well as Er/Pd revealed the existence of compounds in the 70+ atom % R region, which are either iso-compositional or appear in extreme vicinity to the newly observed intermetallics, namely, R_5Pd_{2-x} or $R_{2+x}Pd_{1-x}$ (70.3−71.5 atom % R; **3a**: R = Tb, **3b**: R = Er)[25,42] and R_5Pd_2 (**4**, 71.4 atom % R).[20] All of these, **1**−**4**, are the palladides richest in rare earth metal of these and other rare earth metals; Figure 1 shows a cutout of the respective phase diagrams for comparison, together with the next rare-earth metal poorer compounds, Er_3Pd_2 and Tb_3Pd_2 (66.67 atom % R), on which we have reported recently.[29]

DSC analysis of an Er/Pd = 17:7 mixture that underwent a temperature/time protocol as 1050 °C/2 days →800 °C/7 days → cool to room temperature, revealed an exo/endo thermal effect. The exothermic event peaks at 395 °C and is followed by an endothermic transition peaking at 444 °C

https://dx.doi.org/10.1021/acs.inorgchem.0c01311
Inorg. Chem. 2020, 59, 10802−10812

(Figure 2). This thermal behavior bears some analogy with the supercooled liquid state in amorphous alloys[43] or ionic liquids.[44]

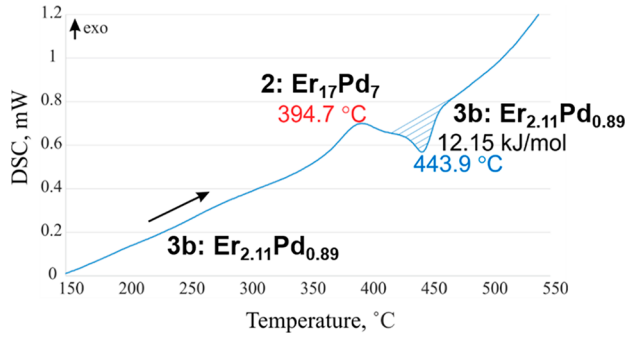

Figure 2. DSC thermogram of a Er/Pd = 17:7 loading after reaction, recorded upon heating (10 °C/min).

X-ray diffraction, both of a single crystal (Tables 1 and 2) and a powder sample (Figure S1), of this reaction shows that after the relatively rapid cooling from 800 °C to ambient temperature, $Er_{2.11}Pd_{0.89}$ (**3b**), 70.3 atom % Er, had formed instead of the targeted $Er_{17}Pd_7$ (**2**). This result is in unison with all the older findings, where compositions of R_5Pd_{2-x} (**3**, 71.5 ± 1 atom % R)[25,42] and R_5Pd_2 (**4**, 71.4 atom % R)[20] were reported. Thus, the new "nonexisting" $Er_{17}Pd_7$ (**2**) can either only be made through the erbium chloride flux routine or is a low-temperature "modification" with a slightly different composition of $Er_{2.11}Pd_{0.89}$ (**3b**), 70.8 versus 70.3 atom % Er, and it undergoes through the combination of an exo/endo phase transformation upon heating to which the DSC analysis hints.

R_5Pd_{2-x} or $R_{2+x}T_{1-x}$ phases and $Er_{17}Pd_7$ have almost identical cubic unit cells although the former are *F*-centered, $Fd\bar{3}m$, while that of $Er_{17}Pd_7$ is primitive, $P2_13$. R_5Pd_{2-x} or $R_{2+x}T_{1-x}$ was reported to have rather substantial positional disorder and to exist for R = Y, Tb−Lu, excluding Yb.[25] R_5Pd_2 (R = Eu and Yb) bear some features of the crystal structure of $Er_{17}Pd_7$ and are isotypic with Pr_5Co_2 and Mn_5C_2. Taking the reported $Pr_{17}Co_7$ into account, this system serves as a bridge combining features of the binary palladide systems from Eu to Lu. While Eu_5Pd_2 was claimed to be isostructural just on the basis of indexing of its powder diffraction pattern,[45] Yb_5Pd_2 was investigated more precisely indicating possible minor Pd deficiency that moves the compound compositionally closer to the nonexisting $Yb_{17}Pd_7$.[46] Finally, R_7Pd_3 type intermetallics were observed for all rare earth elements from La to Gd[47,48] except Eu. Y_7Pd_3 is a special case so far being reported only with at least a minor Gd substitution.[49] Specifically for the Pd series, R_5Pd_2, R_7Pd_3, and $R_{17}Pd_7$ partially complement each other with so far unknown criteria of structural preference.

$R_{17}T_7$ versus $R_{2+x}Pd_{1-x}$. The so-called Dy_5Pd_2 is a representative of complex intermetallics[50] crystallizing in the cubic crystal system with a = 13.529(5) Å.[25] The authors realized that the compound has a composition close to 5:2 but not exactly. Attempts to solve the structure in the high symmetry space group $Fd\bar{3}m$ resulted in a structure description with partial occupancies to avoid unphysically short interatomic distances and R/Pd site mixing. Finally, the authors proposed a point composition $R_{64+4}Pd_{32-4}$ taking into account results from micrographs, DTA (differential thermal analysis) and density measurements.[25] In the most recent single-crystal study[51] a "heavier disorder model" was proposed within the same space group to account for the remaining electron density peaks resulting in a composition of $Dy_{71.17}Pd_{24.48}$, with no further evidence. Moreover, compounds with cubic *F*-centered cells of similar size are relatively popular (~70 representatives) in ternary intermetallics adopting the Dy_4CoCd type of structure. Fortunately, the original publication contained intensity data that allowed to revisit the structure solution. Unfortunately, the data provided do not allow for the confirmation of the authors' space group choice not at least due to missing key reflections (00*l*) and (0*kl*). On the basis of given information, $F\bar{4}3m$ was found to be the most likely space group. Structure solution in the latter led to a positionally ordered structure with partially deficient Pd positions, though the data quality did not allow for an accurate determination of the occupations; however, the solution approaches the initially reported composition. Within this model, the best formula assignment would be Dy_2Pd_{1-x}. Surprisingly, the *ab initio* solution obtained from this restricted data set perfectly matched the structure of the Dy_4CoCd type.[52] Our own investigations of Er/Pd phases in the 70+ atom % Er region revealed single-phase samples (Figure S1). X-ray structure analysis of single crystals of this sample confirmed the initially published structure solution and the existence of at least a minor homogeneity range described by the formula $Er_{2+x}Pd_{1-x}$ with x = 0.11, i.e., $Er_{2.11}Pd_{0.89}$ (**3b**), close in composition to the ordered $Er_{17}Pd_7$, 70.33 versus 70.83 atom % Er. Initial refinement of all occupations resulted in ~50% for Er2, ~89% Pd, and ~11% of Er3 or alternatively ~18% of Pd2 in the same position, so the model with Er/Pd disorder has been chosen as the most appropriate (see Tables 1 and 2). The local disorder in the structure is shown in Figure S2.

The crystal structures of $R_{2+x}Pd_{1-x}$, the Dy_4CoCd type and $R_{17}Pd_7$ phases are linked through group-subgroup relations within the symmetry tree $Fd\bar{3}m - F\bar{4}3m - F23 - P2_13$ (Figure S3), and to some extent reminisce a symmetry relation between Pr_3Pt_{2-x} and Pr_3Pt_2.[53] For comparison with the Dy_4CoCd type, we consider Gd_4PdCd[54] as the chemically closest example. $Er_{17}Pd_7$ (**2**) and Gd_4PdCd are best represented in terms of Heusler type packing assuming all atoms in the latter are substituted by corresponding polyhedra, which are slightly different for both compounds (Figure 3). In contrast to the classical $AlCu_2Mn$ arrangement[55] the current models are better described with its ordered, close relative $CuHg_2Ti$.[56] In stoichiometric **2**, empty Er octahedra occupy two positions of Hg at (0,0,0) and (3/4,3/4,3/4), where the latter fill half of the tetrahedral voids of the initial Er_6 fcc packing (Figure 3, orange and blue, respectively). All octahedral voids of this packing are filled with Er_2Pd_3 trigonal bipyramids (purple), while the remaining half of the tetrahedral voids are occupied by slightly distorted Er_4Pd_4 tetrahedral stars (green). Trigonal bipyramids and tetrahedral stars share a single Er position (Er1, 4*a*). Somewhat elongated thermal ellipsoids of the latter point toward a split position, which can perfectly be explained by stereochemical reasons. A minor shift of that position is required in order to remove the tetrahedral star distortion; however, it would lead to the distortion of the bipyramid. From another point of view, this Er position is close to the center of a Pd_6 trigonal antiprism. There is a strong local force attracting it to the center, but stronger Er−Pd bonding within the bipyramid prevents such a move.

https://dx.doi.org/10.1021/acs.inorgchem.0c01311
Inorg. Chem. 2020, 59, 10802−10812

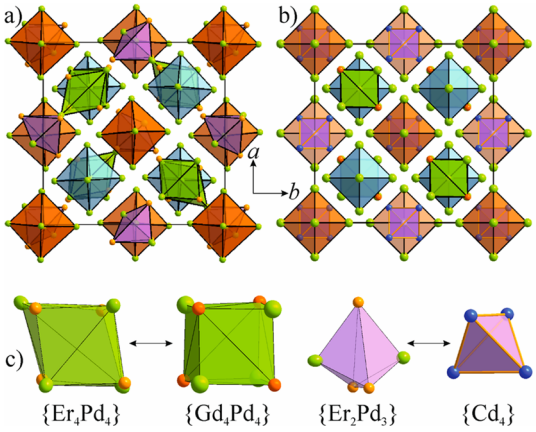

Figure 3. Heusler-type polyhedral packing in the crystal structures of (a) $Er_{17}Pd_7$ and (b) Gd_4PdCd. (c) Polyhedra filling the tetrahedral voids of the Heusler-type packing in the structures of **2** and Gd_4PdCd. Er and Gd atoms are green, Pd atoms are orange, and Cd atoms are blue.

The higher symmetric Gd_4PdCd represents an identical packing of slightly different, more regular polyhedra. Gd_6 octahedra build an *F*-centered cubic arrangement where half of the tetrahedral voids are filled by identical Gd_6 octahedra. The remaining tetrahedral voids correspond to nearly ideal Gd_4Pd_4 tetrahedral stars, while the octahedral voids are filled by Cd_4 tetrahedra (Figure 3). While the octahedral units remain practically identical in both structures, the change of the other polyhedra between both structures is visualized in Figure 3c. Small but visible changes are responsible for the symmetry reduction in **2** compared to that in the Dy_4CoCd type. R_6 octahedra in Gd_4PdCd are oriented parallel to the crystallographic axes: Tetrahedral stars are almost ideal in spite of two different atom types, d_{Pd-Pd} less than 5% longer than d_{R-R}, and finally Pd_4 tetrahedra that substituted Pd_3 triangles are now well-separated from the tetrahedral stars. Due to higher symmetry, $Er_{2.11}Pd_{0.89}$ (**3b**) does not support this concept anymore, and its structure is best described as two non-overlapping networks of empty vertex-sharing Er_6 octahedra and centered edge-sharing $ErPd_6$ octahedra similar to the Ti_2Ni structure type.[57] The chemical separation of the transition metal position into a d−p pair in the ternary compound allows simultaneously higher symmetry and a highly ordered crystal structure.

Another description of the whole series is based on space-filling Pd-centered R polyhedra (Figure 4). The entire structure of $Er_{17}Pd_7$ (**2**) can be divided into two groups of such polyhedral conglomerates based on four edge-sharing $Pd@Er_{6+3}$ = $\{PdEr_{6+3}\}$ tricapped trigonal prisms around an empty Er_4 tetrahedron and $\{Pd_3Er_{20}\}$ anti-Mackay type polytetrahedral clusters based on three interpenetrating icosahedra (Figure 4d,e). Considering Pd_3Er as the cluster core results in a slightly distorted classical 26 atom γ-brass cluster $\{Pd_3Er@Er_{22}\}$ consisting of four prisms: Three of the prisms are symmetrically equivalent and exhibit slightly different upper and lower bases, while the last one is symmetrically restricted and therefore ideal. Each of the trigonal prisms forming these tetramers share all outer vertices with three neighboring tetramers forming an empty Er_6 octahedron (Figure 4a). The crystal structure of Gd_4PdCd contains similar tetramers with all $\{PdGd_6\}$ prisms being equivalent and ideal, but the polytetrahedral clusters are now

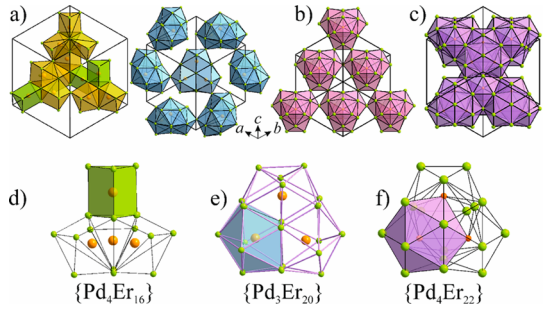

Figure 4. Packing of $\{Pd_4Er_{16}\}$, $\{Pd_3Er_{20}\}$, $\{Cd_4Gd_{22}\}$, and $\{Pd_4Er_{22}\}$ in the crystal structures of $Er_{17}Pd_7$ (a), Gd_4PdCd (b), and $Er_{2.11}Pd_{0.89}$ (c). Construction of the metal clusters in the crystal structure of $Er_{17}Pd_7$ (d, e) as well as Gd_4PdCd and $Er_{2.11}Pd_{0.89}$ (f). Pd and Cd atoms are orange, while Er and Gd atoms are green.

built around the Cd_4 tetrahedron (Figure 4f). These clusters consist of four interpenetrating $\{CdGd_{12}\}$ icosahedra resulting in $\{Pd_4Gd_{22}\}$. The connection of prismatic tetramers remains identical (vertices-based) leading to the analogous empty Gd_6 octahedra in the intercluster space (Figure 4a).

The situation in (**3b**) is significantly different as the higher symmetry, $Fd\bar{3}m$ instead of $P2_13$, leads to the fusion of these two types of conglomerates. The whole structure consists of $\{Pd_4Er_{22}\}$ icosahedral clusters (Figure 4f) sharing a good number of smaller trigonal faces with identical units. The capped $\{PdEr_6\}$ trigonal prisms can be observed inside of the icosahedra although with noticeably different upper and lower trigonal faces. Since the packing of large icosahedral clusters cannot be dense(st), a decent number of octahedral voids is present in analogy with the two previously described compounds.

$\{TR_6\}$ trigonal prisms and their conglomerates are frequently observed building units in binary rare-earth-metal−transition metal systems. Dimers have been noticed as unique motifs in Pr_4Pt_3 or Pr_3Pt_2.[10,58] This building unit plays also a significant role in the two compositionally related intermetallics R_7Pd_3 and R_5Pd_2, as will be discussed below. Anti-Mackay clusters are generally polytetrahedral formations, the most stable of them (at least in the gas phase)[59] consist strictly of interpenetrating icosahedra. Homoatomic dimers of Li icosahedra have been observed in $Sr_{19}Li_{44}$, $Ba_{19}Li_{44}$, $Li_{33.3}Ba_{13.1}Ca_3$, and $Li_{18.9}Na_{8.3}Ba_{15.3}$,[60−62] while Li tetramers exist in $Li_{13}Na_{29}Ba_{19}$.[63] Diatomic dimers, tetramers, and pentamers have been observed in the Mn_3Al_{10} (2),[64] various γ-brasses (4)[65] or in the La−Ni−Mg system (4 and 5).[66] The Bergman cluster consists of 13 interpenetrating icosahedra and is common for Bergman type 1/1 approximant structures.[67] Though trimers and heptamers were predicted to be stable, we could not observe any of them in intermetallic compounds. $Er_{17}Pd_7$ together with $Pr_{17}Co_7$ are the first cases containing trimers with clear chemical separation of the icosahedral centers in analogy with tetramers and pentamers in the La−Ni−Mg system.

R_7T_3 versus R_5T_2. Another system where the halide flux helped to uncover a new phase is Tb/Pd. Tb_7Pd_3 has been obtained through long annealing of an 8Tb + 4$TbCl_3$ + 3Pd mixture, targeting at $\{PdTb_4\}Cl_4$ which was not observed at 650 °C and slow cooling to room temperature. The crystal structure of Tb_7Pd_3 is that of the Th_7Fe_3 structure type. It contains building blocks which are also observed for $Er_{17}Pd_7$ but form different arrangements (Figure 5a). In contrast to

https://dx.doi.org/10.1021/acs.inorgchem.0c01311
Inorg. Chem. 2020, 59, 10802−10812

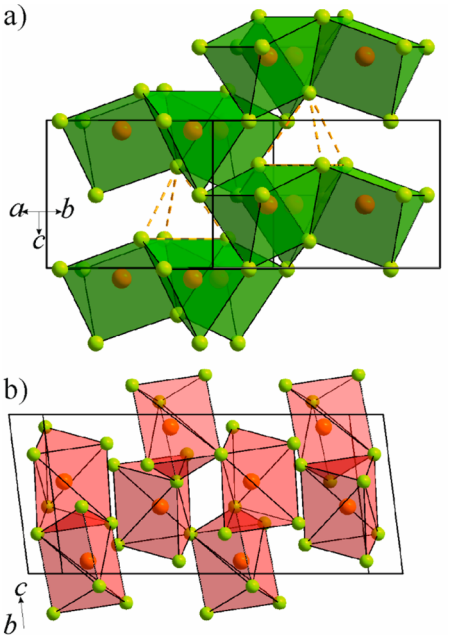

Figure 5. Trigonal prismatic {PdR_6} polyhedra in the crystal structures of Tb_7Pd_3 and Eu_5Pd_2. Tb and Eu atoms are green, and Pd atoms are orange.

$Er_{17}Pd_7$, Pd-centered Tb_6 trigonal prismatic clusters, {$PdTb_6$}, are the exclusive units establishing the entire structure (Figure 5, green), while larger polyicosahedral clusters are completely missing. The {$PdTb_6$} units form edge-sharing trimers around an empty Tb_4 tetrahedron (Figure 5, dashed lines) similar to **2** and **3a** and connect to each other through additional sharing of all outer vertices. All inner vertices participate in the formation of smaller polytetrahedral motifs along the *c*-axis. In contrast, vertex-sharing leads to the formation of octahedral voids surrounded by six trigonal prisms in contrast to four in $Er_{17}Pd_7$ and $Er_{2.11}Pd_{0.89}$ (**3b**, 70.3 atom % Tb).

The R/Pd phases around 29 atom % Pd, R_5Pd_2 (R = Eu and Yb), analogously contain {PdR_6} trigonal prisms as the unique building unit with its own arrangement (Figure 5b). They crystallize in the monoclinic Mn_5C_2/Pd_5B_2 structure type which exhibits the next step of distortion in the discussed family. The crystal structure consists of double zigzag chains of the mentioned prisms along the *c*-axis in the *bc*-plane sharing edges of the rectangular faces along and between. The last parallel edge is checkered up and down showing an analogy with the $HfCuSi_2$ type.[68] The vertices of these edges are shared between the above and below lying chains. In the space between the chains, we can only outline the empty R_4 tetrahedra and R_5 square pyramids with larger polytetrahedral motifs already missing as a logical consequence due to distortion/symmetry reduction.

Being nearly identical in the whole concentration range, the Tb/Pd and Er/Pd systems exhibit surprisingly different behavior around 29 atom % Pd resulting in the formation of a Th_7Fe_3 structure representative for R = Tb. The discovery of Tb_7Pd_3 by crystal growth from a $TbCl_3$ melt opens further questions as "Where does the change of formation from R_7Pd_3 and $R_{17}Pd_7$ occur?" and "Can they coexist?". The lower temperature parts of these systems have never been investigated in detail and the answer to these questions would require thorough and targeted research, which was not the purpose of the current work. Since many heavy rare-earth−palladium systems show nearly identical thermal behavior, for the remaining R between Tb and Lu intermetallics of one or both of these types are highly probable to exist. No compounds in that area have been reported for either T = Pt or Ni with any of the trivalent rare earths following Gd. This suggests that in other R−T systems, $R_{17}T_7$ or R_7T_3 phases can be hidden or obscured.

The structure type preference between Th_7Fe_3 and Mn_5C_2 strongly depends on the transition metal (Table 3) pointing at the domination of electronic over geometric factors. For example, R_7Rh_3 were observed for nearly all trivalent rare earths from La to Lu, while Ni, Pt, and Ir have been reported only with the light rare earth metals. However, the Mn_5C_2 type is predominant for R_5Ru_2 and R_5Ir_2 but restricted to certain divalent cations with Pd, Pt, and Rh. The La−Ir and Pr−Ir systems were, surprisingly, reported to contain both these types for a limited number of light rare earth metals. In general, it looks as if in spite of a limited number of known representatives, the same two of the four structure types can form in the same R−T system. This observation leads to the conclusion that geometric factors such as atomic size ratios, which are often taken as a guideline whether a certain structure can be expected to form in a system, may not be the appropriate criterion for prediction. Rather, subtle electronic and perhaps thermodynamic factors play an important role. Considering that the covalent radii of Rh and Ir are nearly identical while Ru is a bit larger,[69] the structure type preference

Table 3. Overview of the Compounds and Their Structures Observed around 70 atom % R in the R/T Binary Systems[a]

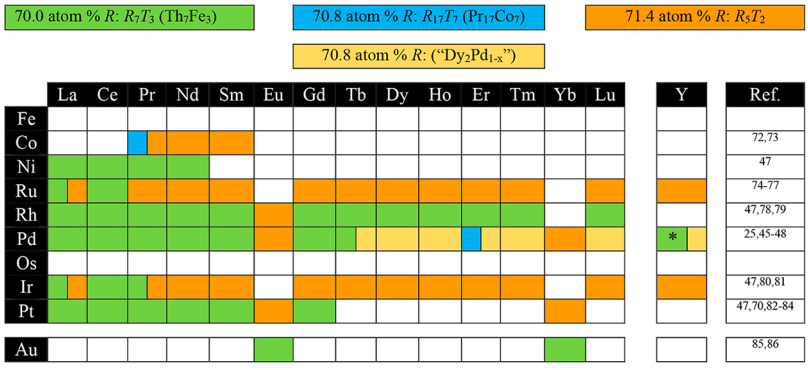

[a]* denotes data reported with minor Gd doping.[49]

https://dx.doi.org/10.1021/acs.inorgchem.0c01311
Inorg. Chem. 2020, 59, 10802−10812

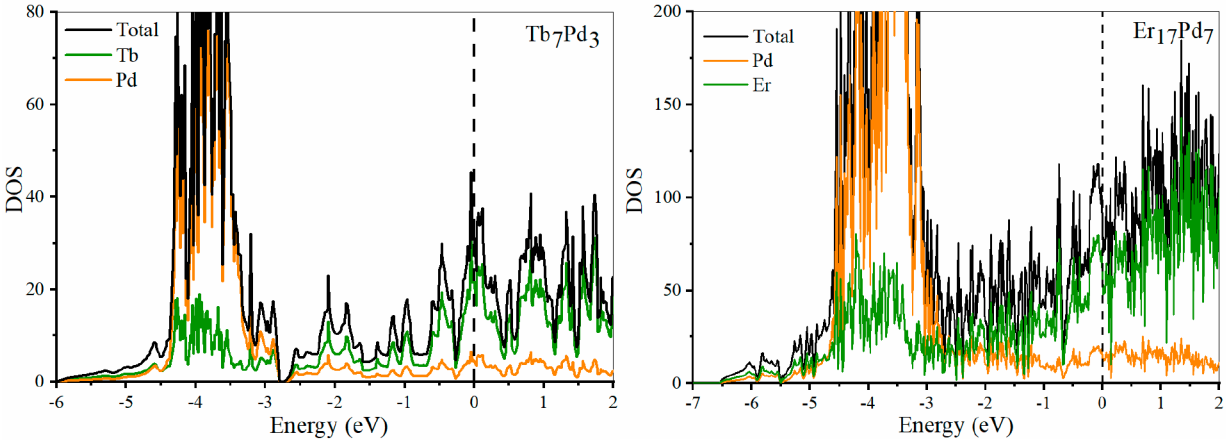

Figure 6. DOS curves for Tb_7Pd_3 (left) and $Er_{17}Pd_7$ (right).

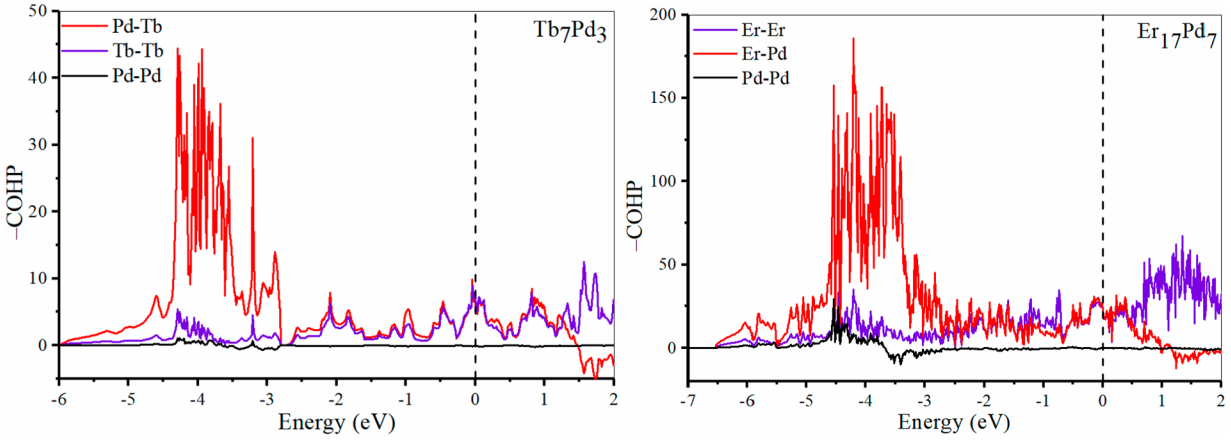

Figure 7. −COHP curves for the interatomic interactions in the crystal structures of Tb_7Pd_3 (left) and $Er_{17}Pd_7$ (right).

looks totally unreasonable, especially when considering the quite large radii range from La to Lu. However, the Th_7Fe_3 type does not exist for Y/Pd unless a minor amount of Gd is added,[49] but it is known for Y/Pt.[70] The Mn_5C_2 type instead may exhibit features of electronic compounds being identified either with predominantly divalent cations for Pd, Pt, and Rh or trivalent with Ru and Ir. Unfortunately, an exact valence electron count for these transition metals is rather problematic to make more precise conclusions. This problem was well-covered in a recent review paper.[71] However, no general elegant solution has been found yet, and every single case requires detailed analysis of the corresponding electronic structures.

Electronic Structure. Calculations have been performed for the two newly discovered compounds, Tb_7Pd_3 and $Er_{17}Pd_7$, in order to uncover features responsible for the structural preference between the corresponding types. The electronic densities of states (DOS) curves for both structures are qualitatively similar over the entire range, with just a few distinct differences. Similar to the binary platinides, they exhibit broad valence bands starting from −6.5 eV for **1** and 6 eV below the Fermi level (E_F) for **2**. Pd 4d states are mainly observed between 3 and 4.5 eV below the Fermi level (Figure 6). They are located slightly above the usual position for 5d orbitals in Au polar intermetallics[87] and below the 5d orbitals of Pt in similar formations.[10] Again, as for platinides, their position well below E_F allows the assignment of formally filled 4d orbitals in valence electron counting approximations. This situation differs from what is observed in ternary platinides with p elements where usually a wider distribution of the transition metal d orbitals is observed.[88−90] Additional contributions from Pd s orbitals are nearly negligible, especially at E_F (Figures S4 and S5), in contrast to the ionic platinides Cs_2Pt or Cs_9Pt_4H.[91,92] Pd 5p contributions become visible and comparable to 4d starting at 2 eV below the Fermi level. Qualitatively similar behavior has also been observed for Tb and Er 6s and 6p below −3 eV. The contributions of R d-states between −6.5 to 3.5 eV are rather small, and they contribute more strongly from 3.5 eV up confirming the view of the compounds as polar intermetallics. This is also supported by COHP analysis (Figure 7).

Both compounds exhibit rather significant DOS values and very narrow local minima at E_F. Large contributions at the Fermi level are mainly due to Tb and Er 5d orbitals strongly dominating above −2 eV. It is interesting to note that narrow but much deeper pseudogaps are observed at ∼0.25 and ∼0.65 eV below the actual Fermi levels for **1** and **2**, respectively. In the case of Tb_7Pd_3 this corresponds to the difference of $3e^-$ per formula unit. Since establishing the actual valence electron count (vec) for the transition metals is not easy, for classical electron counting rules, it is usually accepted as 0. The possible way to reduce vec comes in the actually discovered structure type representatives with divalent cations and gold, e.g., Eu_7Au_3.[85] This is also a possible but so far experimentally

https://dx.doi.org/10.1021/acs.inorgchem.0c01311
Inorg. Chem. 2020, 59, 10802−10812

undiscovered option for **2**. We have shown in our previous work on the example of Pr_3Pt_2 and Pr_3Pt_{2-x}[10] that high-temperature formation is energetically unfavorable, and the structure is being stabilized through the appearance of partially unoccupied positions. This is most likely the case for $Er_{17}Pd_7$ and the disordered $Er_{2.11}Pd_{0.89}$. The change of the electronic structure through the substitution of Pd with a p element has also been proven as an efficient way of the structural stabilization and ordering. It is important that the electronic structure calculation of the isostructural Nd_7Pd_3 with the 4f orbitals included in the calculation does not only show a qualitatively similar electronic structure with large DOS values around the Fermi level but further confirms their negligible role in the bonding interactions.[93]

Distances and Bonding Analysis. In spite of high symmetry, the Er−Pd distances in $Er_{17}Pd_7$ are distributed over a wide range from 2.799(2) to 3.678(2) Å due to the high diversity of structural fragments. We have analyzed the two main building units, the trigonal prisms and the anti-Mackay cluster in more detail. The corresponding distances within the trigonal prisms are 2.799(2) and 3.029(2) Å, while capping extra Er positions in the second coordination sphere may reach up to 4.051(2) Å and can hardly be considered bonding. Er−Pd contacts within the anti-Mackay clusters range from 2.846(2) to 3.678(2) Å with the shortest ones being around the cluster axis, 2.846(2)−2.903(2) Å. The contributions from the shortest Er−Pd "bonds" may reach up to 1.4 eV/bond, while those closer to the upper end are much less populated giving around 0.1−0.3 eV/bond. All Er−Pd interactions under 3.7 Å appear to be bonding resulting in a strongly positive average bonding pattern (Figure 7, Table S1) and a 71% contribution to the total bonding. Pd−Pd contacts in the structure are rare and unusually long, 3.923(3) Å, within the icosahedral trimers and 3.245(3) and 4.250(3) Å within the prismatic tetramers. Even though some of them are close to the sum of the corresponding atomic radii these contacts are nonbonding and are optimized well below the Fermi level. The shortest bonds still show pretty high −ICOHP values of 0.42 eV/bond. As a result, their interactions provide a minor 2% in the total bonding. Er−Er contacts are enclosed in a pretty narrow region between 3.33 and 3.72 Å. Showing the smallest contribution per bond, they dominate quantitatively over the entire structure and provide 27% to the total bonding and, as a rule, 0.1−0.3 eV/bond. The COHP curves show that both Er−Pd and Er−Er contacts are strongly bonding at E_F, while adding more valence electrons moves the system into less bonding areas, although not into antibonding regions. Removing valence electrons is more favorable and slightly enhances the bonding interactions.

Since the majority of positions in the crystal structure of $Er_{2.11}Pd_{0.89}$ are positionally disordered, we analyze the slightly idealized model with an average coordinate for Er2 leading to a fully occupied position at (1/2, 1/2, 1/2) and assuming fully occupied Pd positions. The situation in both structures is quantitatively similar but qualitatively different due to the variation of the distances. The enhanced symmetry leads to smaller diversity of bond lengths and their narrower distribution. Pd−Pd distances are restricted to just one value, 3.74 Å, yielding even smaller and nearly negligible Pd−Pd bonding contributions as compared with those of $Er_{17}Pd_7$. The Er−Er distance range is similar, 3.44−3.55 Å, and no longer continuous with three clearly different lengths. Much more interesting is the Er−Pd distance range, even without considering the disorder. The absolute electronegativities of palladium and rare earth metals are closer to each other compared to platinum, resulting in less extreme polar interactions. It is, however, evident that Er states are involved in bonding with Pd 4d at somewhat lower energies, 3−5 eV below the Fermi level. Such overlap is rather usual for rare earth metal polar intermetallics with Pt or Au and post transition elements.[88−90,94,95] Since there is just one building block in the structure, polyicosahedral $\{Pd_4Er_{22}\}$ clusters, the variety of possible Er−Pd contacts is limited to 2.88, 3.03, and 3.42 Å, significantly simplified compared to $Er_{17}Pd_7$. Taking into account real coordinates of the Er split positions, one further distance of about 2.68 Å may exhibit an insignificant shortening compared with $Er_{17}Pd_7$ but is in good agreement with the minor deficiency of the Pd position.

Not surprisingly the bonding picture in the compositionally related Tb_7Pd_3 is qualitatively and quantitatively similar to the previously discussed compounds (Figure 7, Table S2). Both Tb−Pd and Tb−Tb COHP curves show strong bonding interactions at the Fermi level, while Pd−Pd interactions are negligible. Decent addition or subtraction of valence electrons shift those interactions into a less bonding area. Tb−Pd contacts are located in the narrow range between 2.85 and 2.94 Å covering the distances within the trigonal prisms and providing 0.82−1.02 eV/bond. Formally we also need to consider "bonds" in the second coordination sphere of Pd, which include the Tb atoms capping the rectangular faces. These "bonds", ranging from 3.44 to 3.58 Å, do not contribute significantly to total bonding. All Pd−Pd contacts are longer than 4 Å, while Tb−Tb distances, despite of high symmetry and a small cell, are concentrated between 3.40 and 3.85 Å with the shortest being located formally between four Pd positions and providing 0.09−0.23 eV/bond. The cumulative integrated −COHP values analysis yields an almost 80% contribution to total bonding from the Tb−Pd interactions and almost 20% for Tb−Tb. The small redistribution of the partial contribution is mainly due to the higher proportion of the heteroatomic R−Pd bonds in **1**, 85%, versus those in **2**, 62%, partially compensated by the bigger proportion of short contacts in the latter.

CONCLUSIONS

Two new binary palladides rich in rare earth metal, Tb_7Pd_3 (**1**, 70 atom % Tb) and $Er_{17}Pd_7$ (**2**, 70.8 atom % Er), have been discovered through flux growth from RCl_3 (R = Tb and Er) melts in reactions targeting the cluster complex halides $\{PdR_4\}Cl_4$ which could not be obtained. Reactions without a chloride flux yielded single crystals of $Er_{2.11}Pd_{0.89}$ (**3b**, 70.3 atom % Tb), with a composition that was previously reported for R = Tb−Lu with the exception of Yb. The crystal structure of $Er_{17}Pd_7$ is that of the recently reported $Pr_{17}Co_7$, while Tb_7Pd_3 adopts the Th_7Fe_3 type of structure. Both Tb_7Pd_3 and $Er_{17}Pd_7$ appear to be compositionally approaching or even overlapping with known phases, addressed as $R_{2+x}T_{1-x}$ or R_5T_2. All of these exhibit a variety of structural elements based on one identical unit, a $\{Pd@R_6\}$ trigonal prism. In contrast, various polyicosahedral clusters have been observed in this class of compounds for the first time. $Er_{17}Pd_7$ as well as the ternary structure type Dy_4CoCd were found to be ordered analogues of $Er_{2.11}Pd_{0.89}$, showing that both electronic and thermodynamic factors play a significant role in their stabilization.

https://dx.doi.org/10.1021/acs.inorgchem.0c01311
Inorg. Chem. 2020, 59, 10802−10812

Electronic structure calculations revealed that both compounds are metallic showing narrow local minima at the Fermi level and deeper pseudogaps shifted to lower electron counts. At least one structure type, Th_7Fe_3, features electronic stability ranges (restricted valence electron/atom, *e*/*a*, ratio). The compounds around the composition $R_{17}Pd_7$ are reminiscent of the situation with the two recently discovered platinides Pr_3Pt_2 and Pr_3Pt_{2-x} with thermodynamics being responsible for the compositional and therefore structural changes. The overall bond populations in all structures are significantly dominated by heteroatomic R−Pd interactions with nonbonding Pd−Pd interactions and less populated R−R contacts. Analysis of all known representatives of solely late transition metals with rare earth metals in that narrow composition range show that valence electron count may play a decent role, but the nature of each specific transition metal and thermodynamic aspects are crucial for the structural preference.

■ ASSOCIATED CONTENT

Supporting Information

The Supporting Information is available free of charge at https://pubs.acs.org/doi/10.1021/acs.inorgchem.0c01311.

Powder diffraction patterns, illustration of the disorder within the gamma-brass cluster in the crystal structure of $Er_{2.11}Pd_{0.89}$, group−subgroup schemes for the structures of $Er_{2.11}Pd_{0.89}$ and $Er_{17}Pd_7$, orbital projected DOS curves, augmented binary phase diagrams, interatomic contacts and the corresponding −ICOHP values for **1** and **2** (PDF)

Accession Codes

CCDC 1839878−1839880 contain the supplementary crystallographic data for this paper. These data can be obtained free of charge via www.ccdc.cam.ac.uk/data_request/cif, or by emailing data_request@ccdc.cam.ac.uk, or by contacting The Cambridge Crystallographic Data Centre, 12 Union Road, Cambridge CB2 1EZ, UK; fax: +44 1223 336033.

■ AUTHOR INFORMATION

Corresponding Authors

Anja-Verena Mudring − *Department of Materials and Environmental Chemistry, Stockholm University, 10691 Stockholm, Sweden;* orcid.org/0000-0002-2800-1684; Email: anja-verena.mudring@mmk.su.se

Gerd H. Meyer − *Department of Chemistry, Universität zu Köln, 50939 Köln, Germany; Department of Chemistry, Royal Institute of Technology (KTH), 10042 Stockholm, Sweden;* orcid.org/0000-0003-1000-9001; Email: gerdm@kth.se

Authors

Thomas Bell − *Department of Chemistry, Universität zu Köln, 50939 Köln, Germany*

Volodymyr Smetana − *Department of Materials and Environmental Chemistry, Stockholm University, 10691 Stockholm, Sweden;* orcid.org/0000-0003-0763-1457

Complete contact information is available at: https://pubs.acs.org/10.1021/acs.inorgchem.0c01311

Notes

The authors declare no competing financial interest.

■ ACKNOWLEDGMENTS

Initial research by T.B. was supported by direct funds from the University of Cologne, Cologne, Germany to GHM. More recent research was supported by the Swedish Energy Agency, Energimyndigheten. A.V.M. acknowledges in addition Stockholm University and the Göran Gustafsson Stiftelse/Swedish Royal Academy of Science for support.

■ DEDICATION

Dedicated to Professor Arndt Simon on the occasion of his 80th birthday.

■ REFERENCES

(1) Meyer, G. Reduced halides of the rare-earth elements. *Chem. Rev.* **1988**, *88*, 93−107.

(2) Meyer, G. Symbiosis of Intermetallic and Salt: Rare-Earth Metal Cluster Complexes with Endohedral Transition Metal Atoms. *Handb. Phys. Chem. Rare Earths* **2014**, *45*, 111−178.

(3) Meyer, G. Cluster Complexes as anti-Werner Complexes. *Z. Anorg. Allg. Chem.* **2008**, *634*, 2729−2736.

(4) Meyer, G. Rare Earth Metal Cluster Complexes In *The Rare Earth Elements*; Atwood, D. A., Ed.; John Wiley & Sons, Ltd.: Chichester, UK, 2012; p 415−436.

(5) Rhodehouse, M. L.; Bell, T.; Smetana, V.; Mudring, A.-V.; Meyer, G. H. An Obscured or Nonexistent Binary Intermetallic, Co_7Pr_{17}, Its Existent Neighbor Co_2Pr_5, and Two New Ternaries in the System Co/Sn/Pr, $CoSn_3Pr_{1-x}$, and $Co_{2-x}Sn_7Pr_3$. *Cryst. Growth Des.* **2018**, *18*, 6273−6283.

(6) Massalski, T.; Okamoto, H.; Subramanian, P.; Kacprzak, L. *Binary Alloy Phase Diagrams*; ASM International: Materials Park, OH, 1990.

(7) Provino, A.; Sangeetha, N. S.; Dhar, S. K.; Smetana, V.; Gschneidner, K. A.; Pecharsky, V. K.; Manfrinetti, P.; Mudring, A.-V. New R_3Pd_5 Compounds (R = Sc, Y, Gd−Lu): Formation and Stability, Crystal Structure, and Antiferromagnetism. *Cryst. Growth Des.* **2016**, *16*, 6001−6015.

(8) Nassau, K.; Cherry, L. V.; Wallace, W. E. Intermetallic compounds between lanthanons and transition metals of the first long period: I—Preparation, existence and structural studies. *J. Phys. Chem. Solids* **1960**, *16*, 123−130.

(9) Gilmore, C. M.; Wang, F. E. Note on the structure of $TbFe_2$ and $TbFe_3$. *Acta Crystallogr.* **1967**, *23*, 177−179.

(10) Rhodehouse, M.; Bell, T.; Smetana, V.; Mudring, A.-V.; Meyer, G. From the "non-existent" polar intermetallic Pt_3Pr_4 via $Pt_{2-x}Pr_3$ to some insight into Pt/Sn/Pr ternaries. *Inorg. Chem.* **2018**, *57*, 9949−9961.

(11) Chai, P.; Corbett, J. D. Two new compounds, beta-ScTe and Y_3Au_2, and a reassessment of Y_2Au. *Acta Crystallogr., Sect. C: Cryst. Struct. Commun.* **2011**, *67*, i53−i55.

(12) Celania, C.; Smetana, V.; Mudring, A.-V. Crystal structures and new perspectives on Y_3Au_4 and $Y_{14}Au_{51}$. *Acta Crystallogr., Sect. C: Struct. Chem.* **2017**, *73*, 692−696.

(13) Provino, A.; Smetana, V.; Paudyal, D.; Gschneidner, K. A.; Mudring, A.-V.; Pecharsky, V. K.; Manfrinetti, P.; Putti, M. Gd_3Ni_2 and $Gd_3Co_xNi_{2-x}$: magnetism and unexpected Co/Ni crystallographic ordering. *J. Mater. Chem. C* **2016**, *4*, 6078−6089.

(14) Ostertag, W.; Strnat, K. L. Rare earth cobalt compounds with the A_2B_{17} structure. *Acta Crystallogr.* **1966**, *21*, 560−565.

(15) Wernick, J. H.; Geller, S. Transition element-rare earth compounds with Cu_5Ca structure. *Acta Crystallogr.* **1959**, *12*, 662−665.

(16) Ostertag, W. The crystal structure of Er_2Co_7 and other rare earth-cobalt compounds R_2Co_7 (R = Gd, Tb, Dy, Ho, Tm, Lu, Y). *J. Less-Common Met.* **1967**, *13*, 385−390.

(17) Buschow, K. H. J. Rare-earth-cobalt intermetallic compounds. *Philips Res. Repts* **1971**, *26*, 49−64.

(18) Harris, I. R.; Mansey, R. C.; Slanicka, M.; Taylor, K. N. R. Rare-earth intermediate phases. The room temperature lattice spacings of some $Gd_{1-x}ErxCo_2$ alloys. *J. Less-Common Met.* **1969**, *19*, 437−440.
(19) Lemaire, R.; Schweizer, J.; Yakinthos, J. Structure cristalline des composes intermetalliques T_4Co_3 (T = Y, Gd, Tb, Dy, Ho, Er et Tm). *Acta Crystallogr., Sect. B: Struct. Crystallogr. Cryst. Chem.* **1969**, *25*, 710−713.
(20) Adams, W.; Moreau, J.-M.; Parthe, E.; Schweizer, J. $R_{12}Co_7$ compounds with R = Gd, Tb, Dy, Ho, Er. *Acta Crystallogr., Sect. B: Struct. Crystallogr. Cryst. Chem.* **1976**, *32*, 2697−2699.
(21) Buschow, K. H. J.; Van Der Goot, A. S. The crystal structure of rare-earth cobalt compounds of the type R_3Co. *J. Less-Common Met.* **1969**, *18*, 309−311.
(22) Takao, K.; Sakamoto, Y.; Araki, T.; Kohzuma, H. Observations of ordered Pd_7RE (RE ≡ Tb, Tm, Yb, Lu) phases in Pd—RE alloys. *J. Alloys Compd.* **1993**, *193*, 41−43.
(23) Erdmann, B.; Keller, C. Actinide(lanthanide)-noble metal alloy phases, preparation and properties. *J. Solid State Chem.* **1973**, *7*, 40−48.
(24) Borzone, G.; Cacciamani, G.; Ferro, R. Systematics of rare earth-palladium alloys: Revision of a few systems and forecast of the tb-pd phase diagram. *CALPHAD: Comput. Coupling Phase Diagrams Thermochem.* **1990**, *14*, 139−149.
(25) Fornasini, M. L.; Palenzona, A. Crystal structure of the so-called $R.E._5Pd_2$ compounds. *J. Less-Common Met.* **1974**, *38*, 77−82.
(26) Palenzona, A.; Iandelli, A. The crystal structure and lattice constants of RE_3Pd_4, Y_3Pd_4 and Th_3Pd_4 compounds. *J. Less-Common Met.* **1974**, *34*, 121−124.
(27) Inagawa, K.; Watanabe, K.; Kaneko, T.; Ido, H.; Watanabe, H. Crystal Structure of RPd (R = Tb, Ho, Yb). *J. Phys. Soc. Jpn.* **1974**, *36*, 1709−1709.
(28) Palenzona, A.; Cirafici, S. Thermodynamic and crystallographic properties of REPd intermetallic compounds. *Thermochim. Acta* **1975**, *12*, 267−275.
(29) Bell, T.; Celania, C. R.; Smetana, V.; Mudring, A.-V.; Meyer, G. Tb_3Pd_2, Er_3Pd_2 and Er_6Co_{5-x}: structural variations and bonding in rare-earth-richer binary intermetallics. *Acta Crystallogr., Sect. C: Struct. Chem.* **2018**, *74*, 991−996.
(30) Meyer, G.; Ax, P. An analysis of the ammonium chloride route to anhydrous rare-earth metal chlorides. *Mater. Res. Bull.* **1982**, *17*, 1447−1455.
(31) Meyer, G.; Garcia, E.; Corbett, J. D. The Ammonium Chloride Route to Anhydrous Rare Earth Chlorides—The Example of YCl_3. *Inorg. Synth.* **2007**, 146−150.
(32) *APEX3*; Bruker AXS Inc.: Madison, WI, 2015.
(33) *SAINT*; Bruker AXS Inc.: Madison, WI, 2015.
(34) Krause, L.; Herbst-Irmer, R.; Sheldrick, G. M.; Stalke, D. Comparison of silver and molybdenum microfocus X-ray sources for single-crystal structure determination. *J. Appl. Crystallogr.* **2015**, *48*, 3−10.
(35) Sheldrick, G. SHELXT - Integrated space-group and crystal-structure determination. *Acta Crystallogr., Sect. A: Found. Adv.* **2015**, *71*, 3−8.
(36) Sheldrick, G. Crystal structure refinement with SHELXL. *Acta Crystallogr., Sect. C: Struct. Chem.* **2015**, *71*, 3−8.
(37) Gelato, L.; Parthé, E. STRUCTURE TIDY−a computer program to standardize crystal structure data. *J. Appl. Crystallogr.* **1987**, *20*, 139−143.
(38) Tank, R.; Jepsen, O.; Burkhardt, A.; Andersen, O. K. *TB-LMTO-ASA Program*; Max-Planck-Institut für Festkörperforschung: Stuttgart, Germany, 1994.
(39) Andersen, O. K.; Jepsen, O. Explicit, First-Principles Tight-Binding Theory. *Phys. Rev. Lett.* **1984**, *53*, 2571−2574.
(40) Lambrecht, W. R. L.; Andersen, O. K. Minimal basis sets in the linear muffin-tin orbital method: Application to the diamond-structure crystals C, Si, and Ge. *Phys. Rev. B: Condens. Matter Mater. Phys.* **1986**, *34*, 2439−2449.
(41) Dronskowski, R.; Bloechl, P. E. Crystal orbital Hamilton populations (COHP): energy-resolved visualization of chemical bonding in solids based on density-functional calculations. *J. Phys. Chem.* **1993**, *97*, 8617−8624.
(42) Loebich, O.; Raub, E. Die Legierungen des Palladiums mit Yttrium, Samarium, Gadolinium, Dysprosium, Holmium und Erbium. *J. Less-Common Met.* **1973**, *30*, 47−62.
(43) Zhang, T.; Inoue, A.; Masumoto, T. Amorphous Zr-Al-TM (TM = Co, Ni, Cu) Alloys with Significant Supercooled Liquid Region of Over 100 K. *Mater. Trans., JIM* **1991**, *32*, 1005−1010.
(44) Galiński, M.; Lewandowski, A.; Stępniak, I. Ionic liquids as electrolytes. *Electrochim. Acta* **2006**, *51*, 5567−5580.
(45) Iandelli, A.; Palenzona, A. The europium-palladium system. *J. Less-Common Met.* **1974**, *38*, 1−7.
(46) Sologub, O.; Rogl, P.; Salamakha, L.; Bauer, E.; Hilscher, G.; Michor, H.; Giester, G. On phase equilibria and crystal structures in the systems Ce−Pd−B and Yb−Pd−B. Physical properties of R2Pd13.6B5 (R = Yb, Lu). *J. Solid State Chem.* **2010**, *183*, 1013−1037.
(47) Olcese, G. L. Crystal structure and magnetic properties of some 7:3 binary phases between lanthanides and metals of the 8th group. *J. Less-Common Met.* **1973**, *33*, 71−81.
(48) Moreau, J. M.; Parthé, E. Ferromagnetic Gd_7Pd_3 and other rare-earth-palladium compounds with non-centrosymmetric Th_7Fe_3 structure. *J. Less-Common Met.* **1973**, *32*, 91−96.
(49) Talik, E.; Oboz, M.; Kusz, J.; Winiarski, A.; Hofmeister, W. Magnetic and transport properties of $Gd_{7-x}Y_xPd_3$ (x = 0−6) system. *J. Alloys Compd.* **2014**, *582*, 718−729.
(50) Ovchinnikov, A.; Smetana, V.; Mudring, A.-V. Metallic alloys at the edge of complexity: structural aspects, chemical bonding and physical properties. *J. Phys.: Condens. Matter* **2020**, *32*, 243002.
(51) Matsushita, Y.; Toyoizumi, S.; Kitazawa, H.; Morita, K.; Tamaki, A.; Kawada, S. *13th International Conference on Quasicrystals (ICQ13), Kathmandu, Nepal, 2013*; Journal of Physics: Conference Series; IOP Science, 2017, Vol. *809*.
(52) Dogan, A.; Rayaprol, S.; Pottgen, R. Structure and magnetic properties of RE_4CoCd and RE_4RhCd (RE = Tb, Dy, Ho). *J. Phys.: Condens. Matter* **2007**, *19*, 076213.
(53) Rhodehouse, M. L.; Bell, T.; Smetana, V.; Mudring, A.-V.; Meyer, G. H. From the Nonexistent Polar Intermetallic Pt_3Pr_4 via $Pt_{2-x}Pr_3$ to Pt/Sn/Pr Ternaries. *Inorg. Chem.* **2018**, *57*, 9949−9961.
(54) Schappacher, F. M.; Rodewald, U. C.; Pottgen, R. Rare Earth-rich Cadmium Compounds RE_4TCd (T = Ni, Pd, Ir, Pt). *Z. Naturforsch., B: J. Chem. Sci.* **2008**, *63*, 1127.
(55) Heusler, O. Kristallstruktur und Ferromagnetismus der Mangan-Aluminium-Kupferlegierungen. *Ann. Phys.* **1934**, *411*, 155−201.
(56) Puselj, M.; Ban, Z. The crystal structure of $TiCuHg_2$. *Croatom Chem. Acta* **1969**, *41*, 79−83.
(57) Yurko, G. A.; Barton, J. W.; Parr, J. G. The crystal structure of Ti_2Ni. *Acta Crystallogr.* **1959**, *12*, 909−911.
(58) Le Roy, J.; Moreau, J.-M.; Paccard, D.; Parthe, E. R_3T_2 compounds (R = rare earth or Y; T = Rh, Pd, Pt) with the rhombohedral Er_3Ni_2 structure type. *Acta Crystallogr., Sect. B: Struct. Crystallogr. Cryst. Chem.* **1977**, *33*, 2414−2417.
(59) Doye, J. P. K.; Wales, D. J. Structural consequences of the range of the interatomic potential A menagerie of clusters. *J. Chem. Soc., Faraday Trans.* **1997**, *93*, 4233−4243.
(60) Smetana, V.; Babizhetskyy, V.; Vajenine, G. V.; Hoch, C.; Simon, A. Double-Icosahedral Li Clusters in a New Binary Compound $Ba_{19}Li_{44}$: A Reinvestigation of the Ba−Li Phase Diagram. *Inorg. Chem.* **2007**, *46*, 5425−5428.
(61) Smetana, V.; Babizhetskyy, V.; Hoch, C.; Simon, A. Icosahedral Li clusters in the structures of $Li_{33.3}Ba_{13.1}Ca_3$ and $Li_{18.9}Na_{8.3}Ba_{15.3}$. *J. Solid State Chem.* **2007**, *180*, 3302−3309.
(62) Smetana, V.; Kienle, L.; Duppel, V.; Simon, A. Synthesis, Crystal Structure, and TEM Analysis of $Sr_{19}Li_{44}$ and Sr_3Li_2: A Reinvestigation of the Sr−Li Phase Diagram. *Inorg. Chem.* **2015**, *54*, 733−739.

https://dx.doi.org/10.1021/acs.inorgchem.0c01311
Inorg. Chem. 2020, 59, 10802−10812

(63) Smetana, V.; Babizhetskyy, V.; Vajenine, G. V.; Simon, A. Li_{26} Clusters in the Compound $Li_{13}Na_{29}Ba_{19}$. *Angew. Chem., Int. Ed.* **2006**, *45*, 6051−6053.
(64) Taylor, M. The crystal structure of Mn_3Al_{10}. *Acta Crystallogr.* **1959**, *12*, 393−396.
(65) Brandon, J. K.; Brizard, R. Y.; Chieh, P. C.; McMillan, R. K.; Pearson, W. B. New refinements of the [gamma] brass type structures Cu_5Zn_8, Cu_5Cd_8 and Fe_3Zn_{10}. *Acta Crystallogr., Sect. B: Struct. Crystallogr. Cryst. Chem.* **1974**, *30*, 1412−1417.
(66) Solokha, P.; De Negri, S.; Pavlyuk, V.; Saccone, A. Anti-Mackay Polyicosahedral Clusters in La−Ni−Mg Ternary Compounds: Synthesis and Crystal Structure of the $La_{43}Ni_{17}Mg_5$ New Intermetallic Phase. *Inorg. Chem.* **2009**, *48*, 11586−11593.
(67) Bergman, G.; Waugh, J. L. T.; Pauling, L. The crystal structure of the metallic phase $Mg_{32}(Al, Zn)_{49}$. *Acta Crystallogr.* **1957**, *10*, 254−259.
(68) Sprenger, H. Die ternären systeme (Titan, Zirkonium, Hafnium)-kupfer-Silizium. *J. Less-Common Met.* **1974**, *34*, 39−71.
(69) Cordero, B.; Gomez, V.; Platero-Prats, A. E.; Reves, M.; Echeverria, J.; Cremades, E.; Barragan, F.; Alvarez, S. Covalent radii revisited. *Dalton Trans.* **2008**, 2832−2838.
(70) Geballe, T. H.; Matthias, B. T.; Compton, V. B.; Corenzwit, E.; Hull, G. W.; Longinotti, L. D. Superconductivity in Binary Alloy Systems of the Rare Earths and of Thorium with Pt-Group Metals. *Phys. Rev.* **1965**, *137*, A119−A127.
(71) Mizutani, U.; Sato, H. The Physics of the Hume-Rothery Electron Concentration Rule. *Crystals* **2017**, *7*, 9.
(72) Moreau, J.-M.; Paccard, D. The monoclinic crystal structure of R_5Co_2 (R = Pr, Nd, Sm) with the Mn_5C_2 structure type. *Acta Crystallogr., Sect. B: Struct. Crystallogr. Cryst. Chem.* **1976**, *32*, 1654−1657.
(73) Rhodehouse, M.; Bell, T.; Smetana, V.; Mudring, A.-V.; Meyer, G. An Obscured or Nonexistent Binary Intermetallic, Co_7Pr_{17}, its Existent Neighbor Co_2Pr_5, and Two New Ternaries in the System Co/Sn/Pr, $CoSn_3Pr_{1-x}$ and $Co_{2-x}Sn_7Pr_3$. *Cryst. Growth Des.* **2018**, *18*, 6273−6283.
(74) Palenzona, A.; Canepa, F. The phase diagrams of the La-Ru and Nd-Ru systems. *J. Less-Common Met.* **1990**, *157*, 307−313.
(75) Palenzona, A. The phase diagram of the Ce-Ru system. *J. Alloys Compd.* **1991**, *176*, 241−246.
(76) Palenzona, A. The crystal structure of the rare earth rich ruthenium compounds R_3Ru and R_5Ru_2. *J. Less-Common Met.* **1979**, *66*, P27−P33.
(77) Sharifrazi, P.; Mohanty, R.; Raman, A. Intermediate phases in some rare earth-ruthenium systems. *Z. MetaIlkd.* **1984**, *75*, 801−805.
(78) Raman, A. Crystal structures of some Ln_3Rh, Ln_7Rh_3 and $LnRh_3$ Phases. *J. Less-Common Met.* **1972**, *26*, 199−206.
(79) Iandelli, A.; Palenzona, A. The phase diagram of the Eu-Rh system. *Rev. Chim. Miner.* **1983**, *20*, 449−455.
(80) Blazina, Z.; Mohanty, R.; Raman, A. Intermediate phases in some rare earth metal-iridium systems. *Z. MetaIlkd.* **1989**, *80*, 192−196.
(81) Le Roy, J.; Paccard, D.; Moreau, J.-M. R_5Ir_2 compounds (R = Pr, Nd, Sm, Gd, Tb, Dy, Ho, Er, Tm, Lu, Y) with the monoclinic Mn_5C_2 structure. *J. Less-Common Met.* **1980**, *72*, P11−P15.
(82) Le Roy, J.; Moreau, J.-M.; Paccard, D.; Parthe, E. Structures of the rare-earth-platinum compounds R_7Pt_3, R_2Pt, R_5Pt_3 and RPt. *Acta Crystallogr., Sect. B: Struct. Crystallogr. Cryst. Chem.* **1978**, *34*, 9−13.
(83) Iandelli, A.; Palenzona, A. The phase diagram of the Eu-Pt system and the valency behaviour of europium and ytterbium intermetallics with platinum. *J. Less-Common Met.* **1981**, *80*, P71−P82.
(84) Iandelli, A.; Palenzona, A. The ytterbium-platinum system. *J. Less-Common Met.* **1975**, *43*, 205−209.
(85) Palenzona, A. The phase diagram of the Eu-Au system. *J. Less-Common Met.* **1984**, *100*, 135−140.
(86) Iandelli, A.; Palenzona, A. The ytterbium-gold system. *J. Less-Common Met.* **1969**, *18*, 221−227.
(87) Smetana, V.; Rhodehouse, M.; Meyer, G.; Mudring, A.-V. Gold polar intermetallics: structural versatility through exclusive bonding motifs. *Acc. Chem. Res.* **2017**, *50*, 2633−2641.
(88) Samal, S. L.; Corbett, J. D. Synthesis, structure, and bonding analysis of the polar Intermetallic phase Ca_2Pt_2Cd. *Z. Anorg. Allg. Chem.* **2012**, *638*, 1963−1969.
(89) Samal, S. L.; Gulo, F.; Corbett, J. D. Cluster Chemistry in Electron-Poor Ae−Pt−Cd Systems (Ae = Ca, Sr, Ba): $(Sr,Ba)Pt_2Cd_4$, $Ca_6Pt_8Cd_{16}$, and Its Known Antitype $Er_6Pd_{16}Sb_8$. *Inorg. Chem.* **2013**, *52*, 2697−2704.
(90) Gulo, F.; Samal, S. L.; Corbett, J. D. Substantial Cd−Cd bonding in Ca_6PtCd_{11}: a condensed intermetallic phase built of pentagonal Cd_7 and rectangular $Cd_{4/2}Pt$ Pyramids. *Inorg. Chem.* **2013**, *52*, 10112−10118.
(91) Karpov, A.; Nuss, J.; Wedig, U.; Jansen, M. Cs2Pt: A Platinide(-II) Exhibiting Complete Charge Separation. *Angew. Chem., Int. Ed.* **2003**, *42*, 4818−4821.
(92) Smetana, V.; Mudring, A.-V. Cesium platinide hydride $4Cs_2Pt{\cdot}CsH$: an intermetallic double salt featuring metal anions. *Angew. Chem., Int. Ed.* **2016**, *55*, 14838−14841.
(93) Mudryk, Y.; Ritter, C.; Paudyal, D.; Provino, A.; Dhar, S. K.; Manfrinetti, P.; Fauth, F.; Pecharsky, V. K. Magnetostructural behavior in the non-centrosymmetric compound Nd_7Pd_3. *J. Phys.: Condens. Matter* **2019**, *31*, 265801.
(94) Provino, A.; Steinberg, S.; Smetana, V.; Paramanik, U.; Manfrinetti, P.; Dhar, S. K.; Mudring, A.-V. Gold in the layered structures of $R_3Au_7Sn_3$: from relativity to versatility. *Cryst. Growth Des.* **2016**, *16*, 5657−5668.
(95) Provino, A.; Steinberg, S.; Smetana, V.; Kulkarni, R.; Dhar, S. K.; Manfrinetti, P.; Mudring, A.-V. Gold-rich $R_3Au_7Sn_3$: establishing the interdependence between electronic features and physical properties. *J. Mater. Chem. C* **2015**, *3*, 8311−8321.

https://dx.doi.org/10.1021/acs.inorgchem.0c01311
Inorg. Chem. 2020, 59, 10802−10812